Some Silicon-Based Heterostructures for Optical Applications

M. WILLANDER,[1,3] Q.X. ZHAO,[1] O. NUR,[1] and Q.-H. HU[1,2]

1.—Physical Electronics and Photonics, Physics Department, Gothenburg University, SE-412 96 Gothenburg, Sweden. 2.—LightLab AB (publ), SE-412 50, Gothenburg, Sweden. 3.—E-mail:mwi@fy.chalmers.se

In this paper, we will present our recent research on the growth and characterization of some Si-based heterostructures for optical and photonic devices. The heterostructures to be discussed are ZnO nanorods on Si, SiO_2, and other substrates such as SiN and sapphire. We will also consider strained $Si_{1-x}Ge_x$/Si heterostructures for Si optoelectronics. The performance and functionality extension of Si technology for photonic applications due to the development of such heterostructures will be presented. We will focus on the results of structural and optical characterization in relation to device properties. The structural characterization includes x-ray diffraction for assessment of the crystallinity and stress in the films and secondary ion mass spectrometry for chemical analysis. The optical properties and electronic structure were investigated by using photoluminescence. The device application of these thin film structures includes detectors, lasers, and light emitting devices. Some of the Si-based heterostructures to be presented include devices emitting and detecting up to the blue-green and violet wave lengths.

Key words: ZnO nanorods, ZnO wires, Si-based, heterostructures, SiGe

INTRODUCTION

The main drawback of Si is its indirect bandgap, which seriously limits its use for optoelectronic circuits. Due to the fact that Si dominates the microelectronics industry, it has been a goal to achieve monolithic integrated Si-based circuits that include optoelectronic components. To overcome this and by using pure Si, some suggestions have been made in the literature. Among them are the use of porous Si,[1] Si nanoparticles embedded into SiO_2 matrix by ion implantation,[2] using Si clusters embedded into SiO_2,[3] and the use of active impurities such as erbium to achieve efficient luminescence in Si.[4] However, the attempts of the use of pure Si gave limited success and it is far from being commercialized. Only limited success of using pure Si was achieved. An example of this is mainly in two types of devices, waveguides and detectors. The first is the successful demonstration of Schottky barrier detectors for wavelengths below 5.5 μm.[5,6] However, due to its bandgap of 1.12 eV, pure Si-based devices cannot yield high efficiency and wide bandwidth in the infrared range of wavelengths. The second is to utilize Si-based circuits for waveguides, mainly by using the silicon on insulator (SOI) technology, in which the light confinement is achieved by total internal reflection via the large refractive index change at the Si-SiO_2 and Si-air interfaces. Technologically, today, there are many mature processes to fabricate SOI with smooth interface. Nevertheless, the use of semiconductor heterostructure engineering has the promise and success to extend the functionality of Si-based device structures to monolithic optoelectronic circuits.

Zinc oxide is a direct bandgap wurtzite-type semiconductor with an energy gap of 3.37 eV at room temperature. Due to its large bandgap, ZnO is an excellent semiconductor material for applications considered for other wide bandgap materials such as GaN and SiC. In addition to this, due to the extreme large exciton binding energy (about 60 meV), the excitons in ZnO are thermally stable at room temperature, and thus, ZnO has significant advantages in optoelectronic applications such as in the ultraviolet (UV) lasing media. Optically pumped stimulated emission has been demonstrated recently in ZnO nanowires[7] and ZnO films.[8,9] Due the low

(Received May 17, 2004; accepted December 31, 2004)

symmetry of ZnO crystal, three free exciton (FE) transitions can be observed in high-quality ZnO materials. Figure 1 shows a typical reflectance spectrum of bulk single-crystal ZnO, measured at 80 K. The exciton transitions are labeled as FE_A, FE_B, and FE_C. A number of investigations on the fabrication of ZnO nanowires have been reported in the literature.[10–15] The traditional problem in ZnO is to obtain p-type conductivity. Recent studies also indicate significant progress in the growth and understanding of p-type ZnO layers.[16–22] These successes suggest the potential of ZnO for applications in electronic and optoelectronic devices in the near future. One-dimensional materials such as ZnO nanowires are of interest due to their importance in basic scientific research and potential technological applications.[23] The ZnO nanowires have potential for applications in laser devices due to their desirable optical properties. Therefore, a detailed understanding of ZnO wires and the influence of impurities on their properties are important. It may be worth noting that ZnO nanorods as well as thin films can be grown or deposited on various substrates including Si.

Pseudomorphic-strained $Si_{1-x}Ge_x$/Si was introduced as a heterostructure by using low-temperature epitaxy.[24,25] The introduction of strained $Si_{1-x}Ge_x$/Si as well as relaxed $Si_{1-x}Ge_x$/Si heterostructure (with high Ge fraction) systems has led to new horizons for Si technology. A recently published book contains extensive and updated information on $Si_{1-x}Ge_x$ technology.[26] Many types of optical detectors have been made possible by the use of this technology. These detectors have either an increase in the detection limit compared to those employing pure Si or they are based on new device concepts that were not possible to achieve by using pure Si.

A summary of the most important types of $Si_{1-x}Ge_x$ detectors is presented here. In addition, we report our recent investigation of the UV emission from ZnO nanowires, grown on sapphire and Si substrates, by using optical spectroscopy in the temperature range of 80–300 K. We find that the room-temperature UV emission from the ZnO wires in our samples contains two different transitions. We then discuss and review some of the important aspects of using strained $Si_{1-x}Ge_x$/Si heterostructures for optical applications.

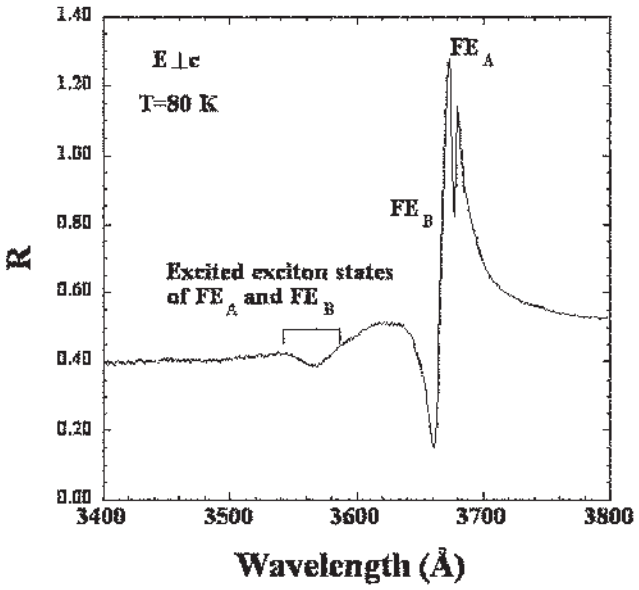

Fig. 1. ZnO reflectivity versus photon wavelength in the exciton region for E perpendicular to the c-axis, measured at 80 K.

GROWTH OF ZnO NANORODS

The ZnO nanorods were synthesized by a vapor-phase transport process using Au nanoparticles as catalyst.[27] In the growth procedure, thin films of Au were deposited on a substrate (1–2 nm), which was then placed in a close vicinity of a mixture of ZnO and graphite powder in a tube furnace. The furnace was heated to about 900°C for 30 min and was then cooled to room temperature in the flow of argon. In this process, ZnO was reduced by carbon; simultaneously, Au film dewetted the substrate and formed nanoclusters. When Zn atoms condensed on Au clusters, Zn formed an alloy with Au temporally and rendered AuZn in a liquid form. Under the catalysis of Au, Zn is oxidized to form ZnO with the Au clusters being elevated on top of the ZnO. Since the lateral growth of ZnO was limited by the size of the Au cluster, thin rods would result as time passed by. The pronounced growth direction was <0001>. The orientation of the rods with respect to the surface of the substrate was determined by the orientation relationship of the ZnO<0001> and the crystallographic orientation of the substrate.

In this work, oxidized Si(001), Si(111), sapphire (0001) and (1 1 -2 0), and amorphous SiN membrane were used as substrates for the ZnO nanorod growth. The choice of the Si substrates is made with the intention of integrating the ZnO nanorods with silicon technology. The choice of the sapphire substrate is based on the consideration of obtaining vertical growth of the nanorods. The choice of SiN membrane is made in order to use transmission electron microscopy (TEM) to study the structural properties of individual rods on the substrate. Scanning electron microscopy (SEM) was performed on the ZnO nanorods grown on these substrates. X-ray diffraction of the nanorods on sapphire substrates was performed to determine the physical structure. Figure 2 shows the SEM micrographs of the nanorods grown on patterned sapphire (1 1 -2 0) surface. A signature of the basal plane of the wurtzite structure can be observed in these micrographs. The dark spots on top of the rods are the Au nanoclusters. The average diameter of the rods is about 100 nm and the average length is about 10 μm. Figure 3 shows the x-ray diffraction spectrum of the ZnO nanorods on sapphire (11-20) substrate. The rods are predominantly c-axis oriented on the substrate, as seen from the strong peaks of ZnO <000L> and sapphire <110>. Figure 4 shows the morphology of the nanorods grown on SiN. The insert shows a selected area diffraction pattern with regular spots from a single ZnO nanorod, indicating

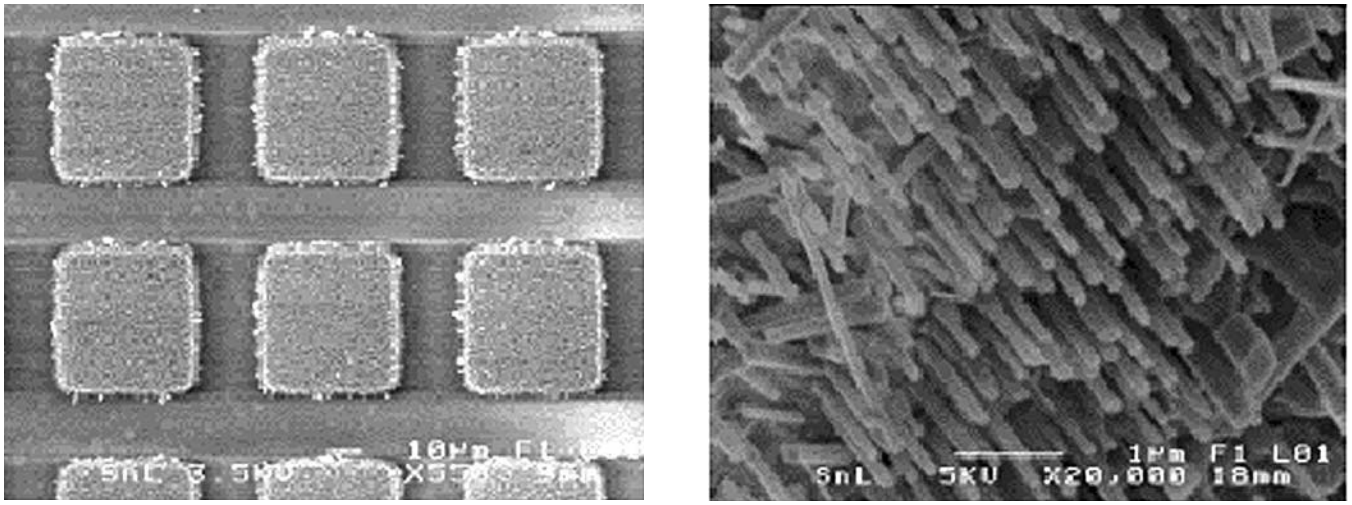

a b

Fig. 2. SEM images of c-axis-oriented ZnO nanowires grown on patterned sapphire (1 1 -2 0) substrate: (a) a top view and (b) a closer view.

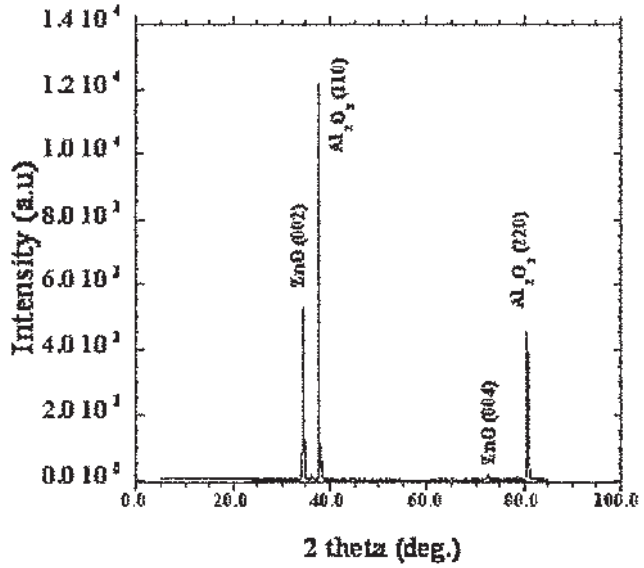

Fig. 3. X-ray diffraction of the ZnO nanorods grown on sapphire (1 1 -2 0); a theta-2theta scan.

single-crystal structure. Other rods appear with different lengths due to different position and tilt during TEM imaging. Photoluminescence spectra of the nanorods were acquired, which reproduced most of the features of the spectra reported in the work of Huang et al.[27] The exception was the lack of appearance of the sharp peaks due to the low power density of our laser. Beyond what they have reported,[27] some of our samples showed strong white-blue emission as witnessed by the naked eye and signified by a broad continuous single peak starting at 4,000 Å and ending at 6,500Å, with the maximum peak height located at about 4,800 Å. The details of photoluminescence (PL) are discussed below in more detail.

OPTICAL CHARACTERIZATION OF ZnO

The ZnO nanowires used in the optical characterization were grown on both sapphire and Si substrates

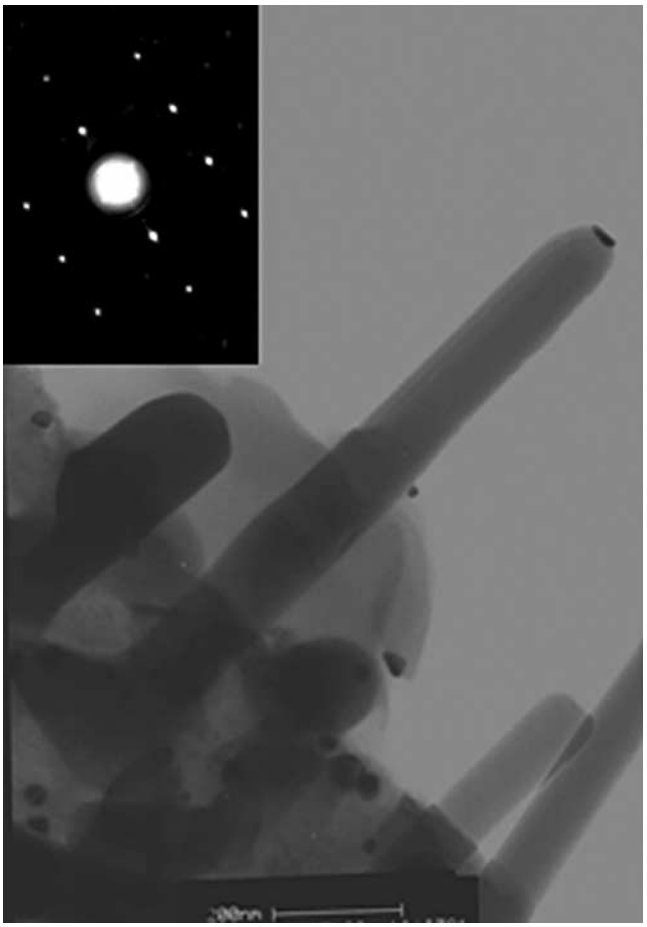

Fig. 4. TEM (a closer look at the individual rods) insert showing the selected area diffraction pattern indicating single-crystal ZnO nanorods; the Au particle is seen on top of the rod.

with a vapor phase transport process, as discussed above. The diameter of the wires can be tuned by controlling the size of the Au particles, whereas the length of the wires can be controlled by the growth time. Figure 2 shows a typical SEM picture of such

ZnO wires investigated in this work. The wires were single crystals, as confirmed by analyzing the x-ray data and by comparison with the results of single-crystal ZnO wires from the literature.[11,13] The average diameter of the wires is about 100 nm and the length is about 5–10 μm. Due to the relatively large diameter of ZnO wires presented here, the quantum confinement effect was not visible in the PL spectra.

The PL measurements were carried out in the temperature range of 80–300 K. A double grating monochromator and a photomultiplier detector were used to disperse and detect the ZnO emission. The laser lines with a wavelength of 270 nm or 350 nm from an Ar^+ laser were used as the excitation sources.

Figure 5 shows the PL spectra of ZnO wires grown on sapphire and Si substrates at a temperature of 80 K. The dominant transitions are the free exciton (FE_A) related to an impurity bound exciton (BE) that is likely due to donor bound excitons and a further intense transition labeled as E_{VI}. By carefully examining the wavelength range longer than the E_{VI} transition, we observed the LO-phonon replicas of the E_{VI} transition with up to three LO phonons involved. In the PL spectrum shown in Fig. 5, only the first LO-phonon replica is clearly visible due to the large intensity scale. The energy separation between the FE_A and E_{VI} is about 60 meV at the temperature of 80 K, and this energy separation decreases with increasing temperature. The ZnO wires grown on sapphire and Si substrates show a similar spectrum, except that the FE_A is relatively stronger in the sample grown on Si substrates, which indicates that the background doping concentration is relatively low. From the PL spectra measured at different excitation power, we can state that at the excitation power used here, none of the observed transitions are related to inelastic exciton-exciton scattering.[7,28–30]

The temperature dependence of the PL spectrum from the ZnO wires grown on a sapphire substrate has been measured and is shown in Fig. 6 in the temperature range from 80 K to 295 K. It clearly shows that the sharp transitions at low temperature develop into a broad band, which is typically observed in ZnO wires and ZnO films.[7,10–15] The PL intensity of both the BE and E_{VI} transitions decreases with increasing temperature, and the transition energy of the BE shows a red shift. Finally, at temperatures around 200 K, the FE_A transition becomes dominant. The red shift of the BE transition is due to the decrease of the ZnO bandgap with increasing temperature. However, the transition E_{VI} shows a different behavior. The transition energy of the E_{VI} is almost unchanged or only slightly red shifted for temperatures up to 150 K. The E_{VI} transition then becomes part of the broad emission band as the temperature is increased to room temperature. This can be seen from the line shape of the PL spectra and from the existence of its LO-phonon replica. Furthermore, the contribution of the E_{VI} transition can be seen in the line shape change of the PL peak at different excitation power. Figure 7 shows the PL spectra measured at room temperature under different excitation powers. The ZnO emission shows a relatively strong red shift with increasing power for the sample on the sapphire substrate in comparison with the ZnO wire sample grown on the Si substrate, due to the different relative strength of the E_{VI} contribution. The FE_A transition is stronger in the ZnO wires grown on the Si substrate than in the ZnO wires grown on the sapphire substrate. This is also observed in the low-temperature PL spectra. From Figure 6, we can see that the wavelength of the UV emission at room temperature from these ZnO wires at low excitation power is about 378 nm with a full-width at half-maximum (FWHM) of 11 nm. This

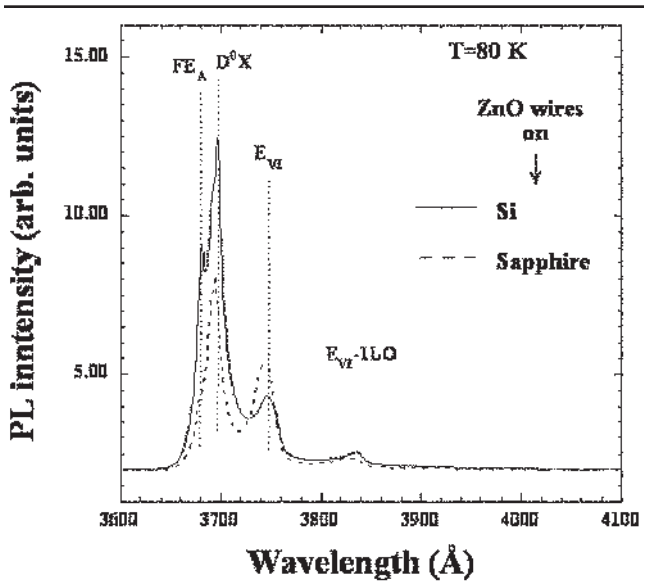

Fig. 5. PL spectra from ZnO wires grown on sapphire and Si substrates, measured at 80 K.

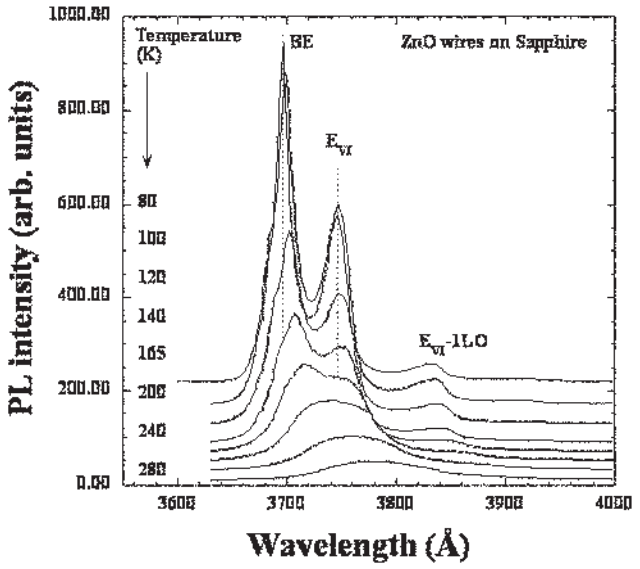

Fig. 6. Temperature dependence of PL spectra from ZnO wires grown on sapphire substrate, measured with excitation wavelength of 350 nm and excitation power of 25 mW.

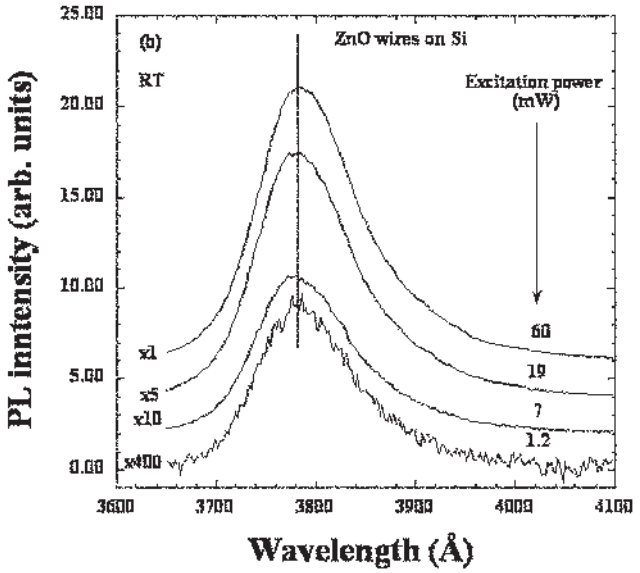

Fig. 7. PL spectra and reflectance spectrum from ZnO wires grown on (a) sapphire substrate and (b) Si substrate, measured at room temperature with three different excitation powers.

indicates that high-quality ZnO wires have been achieved both on Si and sapphire substrates. We note that an emission wavelength of 382 nm with FWHM of 17 nm has been reported earlier in the literature.[7]

The PL spectra for a wide energy range are shown in Fig. 8 at room temperature. In addition to the exciton transition, a broad emission band (white color) appears in the PL spectra. The intensity of the broad emission depends on the growth conditions, as shown in the figure. By choosing proper growth conditions, the intensity of this broad band emission can be manipulated. Therefore, white light emitting diodes can be realized using two methods, one is from the broad emission band and the other is by using excitation of UV exciton emission to excite the white fluoresce materials. Such a device investigation is in progress.

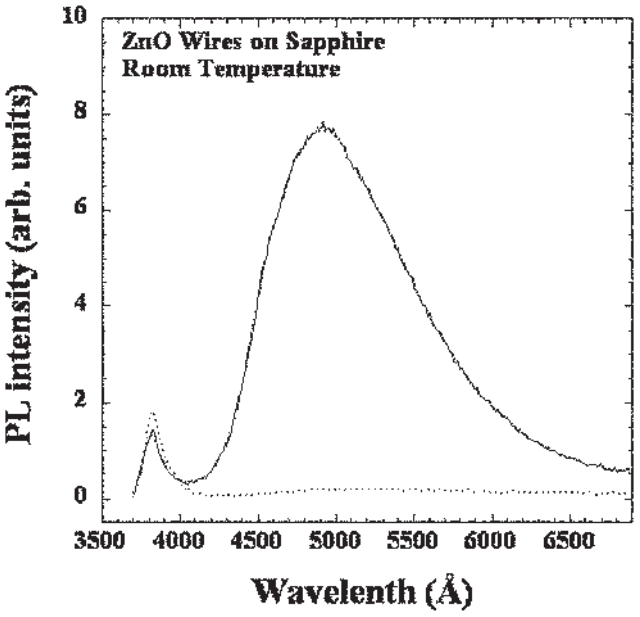

Fig. 8. PL spectra and reflectance spectrum from the ZnO wires grown on sapphire substrate at two growth conditions.

STRAINED $Si_{1-x}Ge_x$/Si FOR OPTOELECTRONICS

PtSi/p-Si Schottky-based contacts have been used commercially as the most mature technology for video cameras imaging at a wavelength below 5.5 μm.[5] The cutoff wavelength of these detectors is defined by the Schottky barrier height. To extend this cutoff wavelength, a barrier height lower than that of PtSi/p-Si is needed. $Si_{1-x}Ge_x$/Si with a reduced bandgap, and especially with most of the band offset lying in the valence band, will easily allow a lower barrier height and consequently extend the cutoff wavelength to 12 μm. Indeed, many reports have demonstrated metal/strained-$Si_{1-x}Ge_x$ Schottky detectors operating in the infrared range of wavelengths.[31–33] In fact, by using a simple metal and the appropriate Ge fraction in the strained-$Si_{1-x}Ge_x$ layer, a barrier height as low as 100 meV can be achieved. Such a barrier will be enough to extend the wavelength to 12-μm infrared radiation. In addition, by using a thin layer of strained-$Si_{1-x}Ge_x$ for the fabrication of the detector with the band offsets at the $Si_{1-x}Ge_x$/Si heterojunction lying in the depletion layer, a bias-dependent detector can be demonstrated. Here, the barrier height is tuned by the applied biasing voltage. This will introduce a variable wavelength detector.

Another category of detectors is the heterojunction internal photoemission (HIP) infrared detectors.[34,35] In an HIP detector, a degenerately heavily doped p-type strained-$Si_{1-x}Ge_x$ layer will be grown on a p-type Si substrate. By degenerately doping the $Si_{1-x}Ge_x$ layers, a strong infrared absorption can be achieved through free carrier absorption and interband transitions. Usually, a doping in excess of 10^{20} cm^{-3} and Ge fraction between x = 0.2–0.4 are needed. The third category of infrared detectors is the strained-$Si_{1-x}Ge_x$/Si quantum well (QW) infrared detectors.[36,37] The mechanism of operation is based on infrared absorption via intervalence sub-band transition of holes in a QW. Usually, in $Si_{1-x}Ge_x$/Si QW infrared detectors, a series of n-type periods of high-quality Si barriers and p-type strained-$Si_{1-x}Ge_x$ wells are grown on high-resistance Si substrates, with the entire structure sandwiched between two thick p-type highly doped Si layers for electrical contacts. The design of these types of detectors should carefully consider the thickness and the Ge fraction in the strained-$Si_{1-x}Ge_x$ well. These parameters should be chosen in a way to obtain a structure with a single bound state and an excited state close to the Si barrier. It is important to note that the absorption of these strained $Si_{1-x}Ge_x$/Si QW infrared detectors is polarization dependent. The absorption is reduced if the angle of the incident beam is increased. This is due to the decrease of the

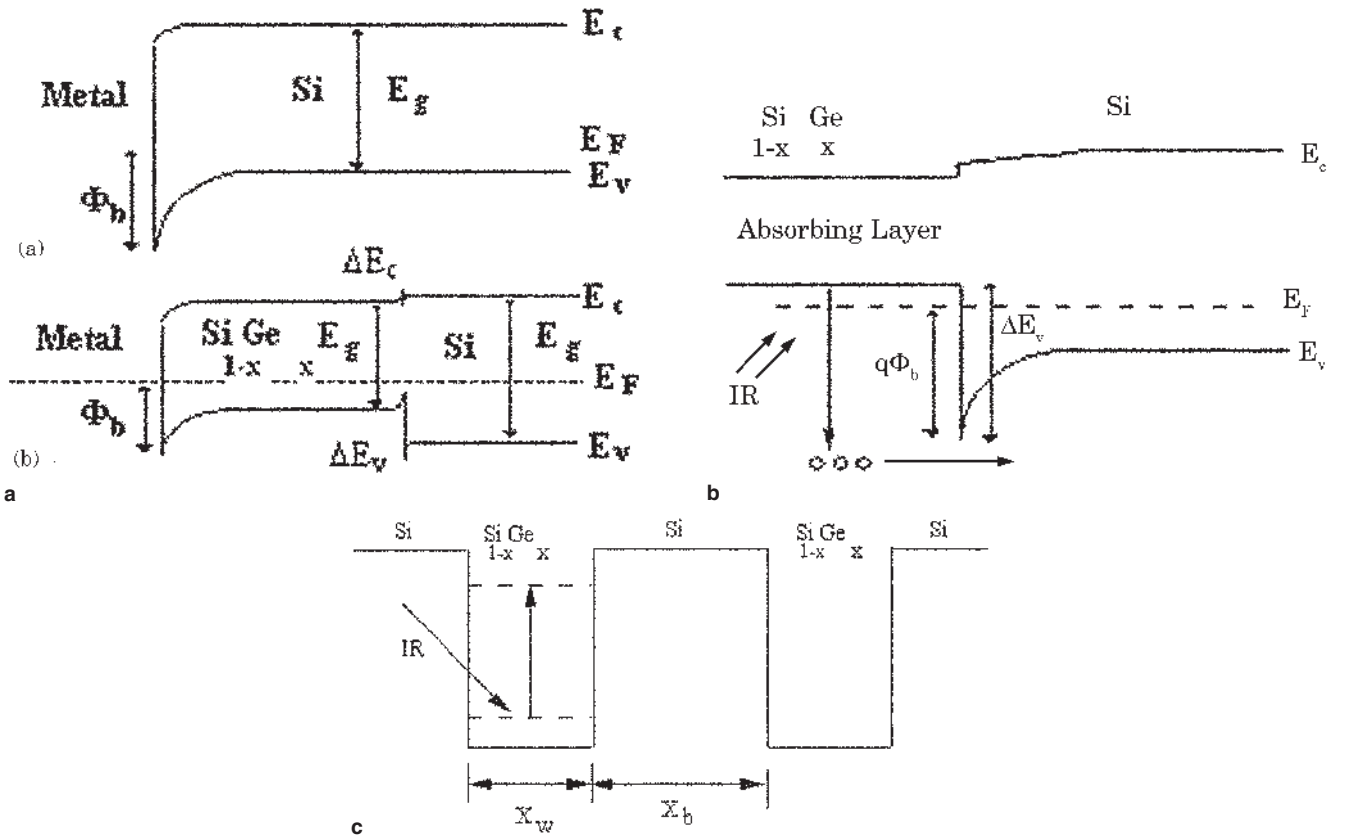

Fig. 9. Schematic energy band diagram of three different strained-$Si_{1-x}Ge_x$ infrared detectors. Top right: Schottky-based detector with extended cutoff wavelength; top left: heterojunction internal photoemission detector, and bottom, strained-$Si_{1-x}Ge_x$/Si QW infrared detector.

electric field in the QW. A schematic energy band diagram of the three above-mentioned detectors is shown in Fig. 9. Relaxed $Si_{1-x}Ge_x$ layers are emerging as candidates to grow high-quality intrinsic Ge thin layers on Si substrates. This is also of technological interest in order to integrate Ge thin layer detectors on Si substrates.

SUMMARY

In summary, high-quality ZnO wires have been grown on Si, SiN, and sapphire substrates. A strong UV emission at a wavelength of 378 nm with FWHM of 11 nm is observed at room temperature. We point out that, due to the relatively large diameter of ZnO wires, the emissions observed in this work are bulk ZnO properties. In order to observe the quantization effect, the diameter of ZnO wires has to be decreased to about tenth nanometers, as illustrated in the ZnO film reported in Ref. 38, in which the bandgap of ZnO depends on the grain size. A brief discussion of the strained and relaxed-$Si_{1-x}Ge_x$ for optoelectronic applications in Si technology is presented. The introduction of strained as well as relaxed-$Si_{1-x}Ge_x$ technology has led to optoelectronic applications of Si monolithic circuits by introducing various types of easily fabricated infrared detectors that were not achievable using pure Si.

REFERENCES

1. V. Lehmann and U. Gösele, *Appl. Phys. Lett.* 58, 856 (1991).
2. H.A. Atwater, K.V. Schhegolv, S.S. Wang, K.J. Vahala, R.C. Flagan, M.L. Brongersma, and A. Polman, *Mater. Res. Soc. Symp. Proc.* 316, 409 (1994).
3. L. Pavesi, L. Dal Negro, C. Mazzoleni, G. Franzo, and F. Priolo, *Nature* 408, 440 (2000).
4. M. Markmann, E. Neufeld, A. Sticht, K. Brunner, G. Abstreiter, and C. Buch Buchal, *Appl. Phys. Lett.* 75, 2584 (1999).
5. K.C. Chenson, B. Nechay, and B.Y. Tsaur, *IEEE Trans. Electron Dev.* 38, 1094 (1991).
6. F.D. Shepherd, *SPIE* 1735, 250 (1992); W.F. Kosonocky, *SPIE* 1308, 2 (1990).
7. M. Huang, S. Mao, H. Feick, H. Yan, Y. Wu, H. Kind, E. Weber, R. Russo, and P. Yang, *Science* 292, 1897 (2001).
8. P. Zu, Z.K. Tang, G.K.L. Wong, M. Kawasakki, A. Ohtomo, H. Koinuma, and Y. Segawa, *Solid State Comm.* 103, 459 (1997).
9. D.M. Bagnall, Y.F. Chen, Z. Zhu, T. Yao, S. Koyama, M. Y. Shen, and T. Goto, *Appl. Phys. Lett.* 70, 2230 (1997).
10. H. Cao et al., *Phys. Rev. Lett.* 84, 5584 (2000).
11. W.I. Park, D.H. Kim, S.W. Jung, and Gyu-Chui Yi, *Appl. Phys. Lett.* 80, 4232 (2002)
12. Hensoo Kim and Wolfgang Sigmund, *Appl. Phys. Lett.* 81, 2085 (2002).
13. Seung Chul Lyu, Ye Zhang, Hyun Ruh, Hwack-Joo Lee, Hyun-Wook Shim, Eun-Kyung Suh, and Cheol Jin Lee, *Chem. Phys. Lett.* 363, 134 (2002).
14. Y.W. Wang, L.D. Zhang, G.Z. Wang, X.S. Peng, Z.Q. Chu, and C.H. Liang, *J. Cryst. Growth* 234, 171 (2002).
15. Sung-Sik Chang, Sang Ok Yoon, Hye Jeong Park, and Akira Sakai, *Mater. Lett.* 53, 432 (2002).
16. D.C. Look et al., *Appl. Phys. Lett.* 81, 1830 (2002).
17. T. Aoki et. al., *Phys. Status Solidi B* 229, 911 (2002).
18. Yanfa Yan, S.B. Zhang, and S.T. Pantelides, *Phys. Rev. Lett.* 86, 5723 (2001).
19. S.B. Zhang, S.H. Wei, and Alex Zunger, *Phys. Rev. B* 63, 075205 (2001).

20. C.H. Park, S.B. Zhang, and S.H. Wei, *Phys. Rev. B* 66, 073202 (2002).
21. T. Aoki, Y. Hatanaka, and D.C. Look, *Appl. Phys. Lett.* 76, 3257 (2000).
22. E.C. Lee, Y.S. Kim, Y.G. Jin, and K.J. Chang, *Phys. Rev. B.* 64, 085120 (2001).
23. J. Hu, T.W. Odom, and C.M. Lieber, *Acc. Chem. Res.* 332, 435 (1999).
24. E. Kasper, H. J. Herzog, and H. Kibbel, *Appl. Phys. Lett.* 8, 199 (1975).
25. E. Kasper, H. J. Herzog, and H. Kibbel, *Thin Solid Films* 44, 357 (1977).
26. S.C Jain and M. Willander, *Silicon-Germanium Strained Layers and Heterostructures, Semiconductors and Semimetals* (New York: Academic Press: 2003), vol. 74.
27. M.H. Huang, S. Mao, H. Feick, Y. Haoquan, W. Wiying, H. Kind, E. Weber, R. Rosso, and Y. Peidong, *Adv. Mater.* 13, 113 (2001).
28. J. M. Hvam, *Phys. Status Solidi B* 63, 511 (1974).
29. C. Kligshirn, *Phys. Status Solidi B* 71, 547 (1975).
30. H.J. Ko, Y.F. Chen, Z. Zhu, and T. Yao, *Appl. Phys. Lett.* 76, 1905 (2000).
31. X. Xiao, J.C. Sturm, S.R. Parihar, S.A. Lyon, D. Meyerhofer, and F.V. Shallcross, *IEEE Electron Dev. Lett.* EDL-14, 199 (1993).
32. H. Kanaya, F. Hasegawa, E. Yamaka, T. Moriyama, and M. Nakajima, *Jpn. J. Appl. Phys.* 28, L544 (1989).
33. D.P. Chu, F.M. Peeters, S. Kolodiniski, and E. Roca, *J. Appl. Phys.* 79, 1151 (1996).
34. T.L. Tin, A. Ksendzov, S.M. Dejewski, E.W. Jones, and R.W. Fathaure, *IEEE Trans. Electron. Dev.* 38, 1131 (1991).
35. T.L. Tin, J.S. Park, E.W. Gones, and H.M. Del Castillo, *IEEE Electron. Dev. Lett.* 15, 103 (1994).
36. R.P. Karunasiri, J.S. Park, Y.J. Mi, and K.L. Wang, *Appl. Phys. Lett.* 59, 2588 (1991).
37. R. Misra, D.W. Greve, and T.E. Schelsinger, *Appl. Phys. Lett.* 67, 2548 (1995).
38. S.J. Chen, Y.C. Liu, J.G. Ma, D.X. Zhao, Z.Z. Zhi, Y.M. Lu, J.Y. Zhang, D.Z. Shen, and X.W. Fan, *J. Cryst. Growth* 240, 467 (2002).